





**Trapping of ultrashort pulses in nondegenerate parametric conversion**A. V. Gorbach <sup>1,2,\*</sup>, M. Roiz <sup>3</sup>, M. Vainio <sup>3,4</sup> and D. V. Skryabin <sup>1,2,†</sup><sup>1</sup>*Department of Physics, University of Bath, BA2 7AY, United Kingdom*<sup>2</sup>*Centre for Photonics and Photonic Materials, University of Bath, BA2 7AY, United Kingdom*<sup>3</sup>*Department of Chemistry, University of Helsinki, P.O. Box 55, FI-00014 Helsinki, Finland*<sup>4</sup>*Photonics Laboratory, Physics Unit, Tampere University, FI-33014 Tampere, Finland*

(Received 9 March 2023; accepted 9 June 2023; published 27 June 2023)

Parametric conversion of ultrashort pulses is a versatile tool in nonlinear and quantum optics. Here, we present a detailed theory and numerical investigation of the phenomenon of the signal and idler trapping by the ultrashort pump pulse in a material with second- and third-order nonlinearities. The trapping regime becomes possible by balancing the characteristic length scales associated with the group-velocity mismatch and second-order nonlinearity, ensuring that signal, idler, and pump pulses propagate with the pump group velocity. We have derived analytical solutions for the trapped states and found that the transition between the broadband coherent and in-coherent signal and idler spectra accompanies the changeover between the trapping and no-trapping regimes. We have also demonstrated the higher-order trapped states, reported a significant boost to conversion efficiency in the trapping regime and considered in detail a particular case of the pump pulse being an optical soliton.

DOI: [10.1103/PhysRevA.107.063515](https://doi.org/10.1103/PhysRevA.107.063515)**I. INTRODUCTION**

Parametric frequency conversion is one of the most fundamental and well-studied nonlinear optical processes, which plays a key role in such applications, as spectroscopy and generation of quantum states of light [1–4]. The physical mechanism underpinning diverse applications of parametric processes is the pump’s instability triggered by either vacuum fluctuations or a weak seed. In both cases, the instability peaks at the phase-matching conditions and generates a pair of signal and idler photons. Over the past couple of decades, applications of ultrashort pulses for parametric conversion have become a widely spread experimental technology [3–13].

At first glance, when dealing with the broadband frequency conversion of ultrashort pulses, one rightfully expects that the group-velocity walk-off should limit the useful propagation distances and conversion efficiency. However, dispersion engineering often allows manipulating the group velocities of different parts of broadband signals to suppress their dispersive spreading and walk-off from the pump. One well-studied realization of such a scenario drives supercontinuum generation in photonic crystal fibers [14–17]. Also, supercontinuum generation via group-velocity matching of the 1- $\mu\text{m}$  pump and its half-harmonic has been recently demonstrated

in thin-film lithium-niobate waveguides [18]. Other examples come from the near-group-velocity-matched four-wave mixing between solitons and dispersive waves [19,20] and photon-pair generation in the pulsed four- and three-wave mixings [21–23]. Similar combinations of group velocities were shown to give a dramatic increase in the efficiency of parametric conversion, which occurred due to suppression of the signal and idler walk-off induced by the femtosecond pump [5–8].

The first theory of pulse trapping in parametric three-wave mixing through the interplay of the group-velocity walk-off and  $\chi^{(2)}$  nonlinearity dates back to 1971 [24]. This not widely known reference should not be confused with the later and quite famous Karamzin-Sukhorukov paper on  $\chi^{(2)}$  solitons due to the balance of diffraction/dispersion and nonlinearity [25,26]. Below, we present detailed theoretical studies of the trapping effect in parametric down-conversion of ultrashort pulses. We demonstrate the trapped states of multiple orders, explore their role in the trapping scenario, and compare the amplified fields’ spectral bandwidth and coherence with and without trapping. A practical example we consider describes frequency conversion of the red pump to the infrared signal and idler in a thin-film lithium niobate waveguide. Although the interplay of group-velocity mismatch and  $\chi^{(2)}$  nonlinearity is the focus of our attention, we also investigate the role of cross-phase modulation induced by the Kerr effect in the last section.

**II. THREE-WAVE MIXING MODEL**

We describe the three-wave mixing of ultrashort pulses in an optical waveguide using the coupled equations for the complex envelopes of the pump  $A_p$ , signal  $A_s$ , and idler  $A_i$

\*a.gorbach@bath.ac.uk

†d.v.skryabin@bath.ac.uk

fields [24]

$$\begin{aligned}
i \partial_z A_p &= \frac{1}{2} \beta_{2p} \partial_{tt} A_p - \gamma_2 A_s A_i \\
&\quad - [\gamma_{3pp} |A_p|^2 + 2\gamma_{3ps} |A_s|^2 + 2\gamma_{3pi} |A_i|^2] A_p, \\
i \partial_z A_s &= -i v_s \partial_t A_s + \frac{1}{2} \beta_{2s} \partial_{tt} A_s - \gamma_2 A_p A_i^* \\
&\quad - [\gamma_{3ss} |A_s|^2 + 2\gamma_{3ps} |A_p|^2 + 2\gamma_{3si} |A_i|^2] A_s, \\
i \partial_z A_i &= i v_i \partial_t A_i + \frac{1}{2} \beta_{2i} \partial_{tt} A_i - \gamma_2 A_p A_s^* \\
&\quad - [\gamma_{3ii} |A_i|^2 + 2\gamma_{3pi} |A_p|^2 + 2\gamma_{3si} |A_s|^2] A_i. \quad (1)
\end{aligned}$$

Here,  $z$  is the propagation distance, and  $t$  is time in the frame comoving with the group velocity of the pump.  $|A_k|^2$  is measured in Watts. Second-  $\gamma_2$ , and third-order  $\gamma_{3\dots}$ , nonlinear coefficients have units of  $\text{m}^{-1} \text{W}^{-1/2}$  and  $\text{m}^{-1} \text{W}^{-1}$ , respectively. Their relation with material parameters and waveguide geometry is detailed in Appendix A.

The pump, signal, and idler fields are centered at frequencies  $\omega_p$ ,  $\omega_s$ , and  $\omega_i$ , respectively,  $\hbar\omega_p = \hbar\omega_s + \hbar\omega_i$ . It is assumed that the three-wave mixing (TWM) process at the carrier frequencies of the pump, signal, and idler fields is phase matched, i.e.,  $\beta_p = \beta_s + \beta_i$ . Here,  $\beta_k = \beta(\omega_k)$ ,  $k = p, s$ , and  $i$ , are the respective propagation constants. Pump, signal, and idler could belong to the same or different transverse mode families. The four-wave mixing (FWM) energy conservation,  $2\hbar\omega_p = \hbar\omega_s + \hbar\omega_i$ , cannot be satisfied simultaneously with the assumed TWM one,  $\hbar\omega_p = \hbar\omega_s + \hbar\omega_i$ , therefore, it is safe to disregard the FWM terms omitted in Eq. (1).

Group velocities are defined as  $1/\beta_{1k}$ , where  $\beta_{1k} = \partial_\omega \beta(\omega)|_{\omega=\omega_k}$ . Group-velocity mismatch (GVM) between signal and pump,

$$v_s = \beta_{1s} - \beta_{1p}, \quad (2)$$

and pump and idler,

$$v_i = \beta_{1p} - \beta_{1i} \quad (3)$$

are the key parameters controlling transition between the trapped and the untrapped states of the parametric generation. For future convenience, we also introduce

$$v_\pm = \frac{1}{2}(v_s \pm v_i). \quad (4)$$

Dispersion coefficients are  $\beta_{2k} = \partial_\omega^2 \beta(\omega)|_{\omega=\omega_k}$ .

To analyze the initial stage of parametric generation, we assume that the signal and idler waves are weak and neglect the terms nonlinear in  $A_s$  and  $A_i$ . Then, Eq. (1) separate to the independent equation for the pump,

$$i \partial_z A_p = \frac{1}{2} \beta_{2p} \partial_{tt} A_p - \gamma_{3pp} |A_p|^2 A_p, \quad (5)$$

and a pair of equations for the signal and idler fields,

$$\begin{aligned}
i \partial_z A_s &= -i v_s \partial_t A_s + \frac{1}{2} \beta_{2s} \partial_{tt} A_s - \gamma_2 A_p A_i^* \\
&\quad - 2\gamma_{3ps} |A_p|^2 A_s, \\
i \partial_z A_i &= i v_i \partial_t A_i + \frac{1}{2} \beta_{2i} \partial_{tt} A_i - \gamma_2 A_p A_s^* \\
&\quad - 2\gamma_{3pi} |A_p|^2 A_i. \quad (6)
\end{aligned}$$

We assume that the pump pulse has the peak power  $P$  and duration  $T$ . Then, the dispersion length  $L_d$ , and nonlinear

(Kerr) length  $L_{3nl}$ , are defined as

$$L_d = \frac{T^2}{|\beta_{2p}|}, \quad L_{3nl} = \frac{1}{\gamma_{3pp} P}. \quad (7)$$

Taking as an example a  $600 \times 500 \text{ nm}^2$  lithium niobate ridge waveguide, see Ref. [27], and selecting pump at  $\lambda_p = 0.685 \mu\text{m}$  in the fundamental TE mode, and signal and idler in the fundamental TM mode at  $\lambda_s = 1.5$  and  $\lambda_i = 1.26 \mu\text{m}$ , we estimate  $\beta_{2p} \approx -2.8 \text{ ps}^2/\text{m}$ ,  $\gamma_2 \approx 200 \text{ W}^{-1/2} \text{m}^{-1}$ , and  $\gamma_{3pp} \approx 7.1 \text{ W}^{-1} \text{m}^{-1}$ . For the practical range of  $T$  between 1 ps and 100 fs this gives the range of  $L_d$  between 30 cm and 3 mm. For  $P$  between 1 W and 1 kW,  $L_{3nl}$  varies between 15 cm and 0.15 mm.

Equations for signal and idler make their own characteristic lengths. We define the GVM length as

$$L_{\text{gvm}} = \frac{T}{\sqrt{|v_s v_i|}}. \quad (8)$$

The above waveguide geometry gives  $v_s \approx 0.016/c$  and  $v_i \approx 0.013/c$ , where  $c$  is the vacuum speed of light. Thus, for  $T$  between 1 ps and 100 fs,  $L_{\text{gvm}}$  varies between 2 cm and 2 mm. Nonlinear length originating in the second-order parametric effect is defined as

$$L_{2nl} = \frac{1}{\gamma_2 \sqrt{P}}, \quad (9)$$

and varies between 5 mm for  $P = 1 \text{ W}$  and 0.1 mm for 1 kW.

### III. TRAPPING EFFECT

#### A. Eigenvalue analysis

In this section, we assume that the waveguide length  $L$  is shorter than  $L_d$  and  $L_{3nl}$  but is much longer than  $L_{\text{gvm}}$  and  $L_{2nl}$ . Therefore, we assume that the pump pulse maintains its shape, peak power, and spectral content,

$$A_p(t, z) = S(t) = \sqrt{P} \text{sech}(t/T), \quad (10)$$

which can be referred to as the stationary pump approximation. This approximation implies that the pump pulse degradation due to energy transfer to signal and idler, dispersion and self-phase modulation are negligible over propagation distances of interest. Furthermore, we disregard the second-order dispersion in the signal and idler equation, and introduce

$$\begin{aligned}
A_s(t, z) &= e^{\lambda z} a_s(t), \\
A_i(t, z) &= e^{\lambda^* z} a_i^*(t), \quad (11)
\end{aligned}$$

so that Eq. (6) reduces to an eigenvalue problem,

$$\lambda \begin{bmatrix} a_s \\ a_i \end{bmatrix} = \begin{bmatrix} -v_s \partial_t & i\gamma_2 S(t) \\ -i\gamma_2 S(t) & v_i \partial_t \end{bmatrix} \begin{bmatrix} a_s \\ a_i \end{bmatrix}. \quad (12)$$

Any eigenvalue  $\lambda$  with a positive real part has physical meaning of parametric gain,  $g = \text{Re}(\lambda) > 0$ , and characterizes the exponential growth rate of the signal and idler fields from noise or a weak seed field.

For the cw pump, i.e.,  $S(t) = \text{const}$ , Eq. (12) can be easily solved analytically, see Appendix B. For a pulsed pump  $S(t)$ , the problem can be fully analyzed only numerically. To perform this, we replaced derivatives in Eq. (12)

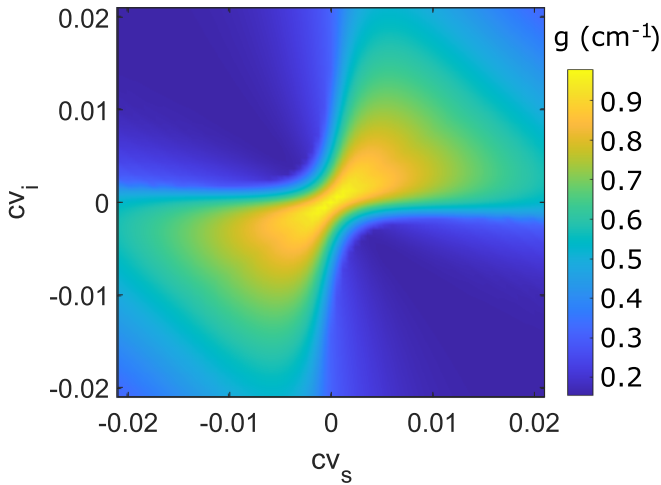


FIG. 1. Maximal gain (in the units of  $\text{cm}^{-1}$ ) as a function of the GVM parameters  $v_s$  and  $v_i$  for the pump pulse peak power  $P = 0.25$  W and width  $T = 0.5$  ps.  $c$  is speed of light in vacuum.

with suitable algebraic approximations and solved the resulting matrix eigenvalue problem using standard linear algebra tools. Figure 1 shows the maximal parametric gain,  $\max g = \max \text{Re}(\lambda)$ , plotted as a function of the GVM parameters  $v_s$  and  $v_i$ , for  $P = 0.25$  W and  $T = 0.5$  ps. The gain function is profoundly asymmetric and much higher in the quadrants with  $v_s v_i > 0$ . This appears to be in stark contrast to the CW pump case where the maximal gain is always equal to  $\max[g^{(\text{cw})}] =$

$\gamma_2 \sqrt{P} = 1 \text{ cm}^{-1}$ , regardless of the combination of  $v_s$  and  $v_i$ , see Appendix B. The gain increases sharply at  $v_i = 0$ , which is directly associated with a qualitative change in the corresponding eigenvectors signaling transition between the trapped and delocalized signal and idler pulses, see Fig. 2.

The  $v_s v_i < 0$  quadrants correspond to the case when the signal-idler pulses are simultaneously slower or faster than the pump. In this case, a typical spectrum contains a quasi-continuous band of eigenvalues with  $\text{Re}(\lambda) > 0$ , see Fig. 2(a). The unstable eigenvectors have narrow quasimonochromatic spectra and are delocalized in time, see Figs. 2(b) and 2(c). The sequence of blue peaks in Fig. 2(b) is obtained by adding spectral profiles of all the unstable eigenvectors with the amplitudes taken proportional to their gain.

For

$$v_s v_i > 0, \quad (13)$$

one pulse from the signal-idler pair is faster, and the other is slower than the pump pulse. The respective quadrants in Fig. 1 have one or few unstable eigenvalues, which are discrete and isolated from the stable continuum, see Fig. 2(d). The unstable eigenvectors are well localized in the time domain, they are both trapped almost in the middle of the pump pulse, which constitutes the essence of the trapping effect of the signal and idler pulses, see Figs. 2(e) and 2(f).

Importantly, Eq. (12) also allows analytical solutions corresponding to the zero order, i.e., fundamental trapped state, see Ref. [24] and Appendix C. Explicit expressions for the

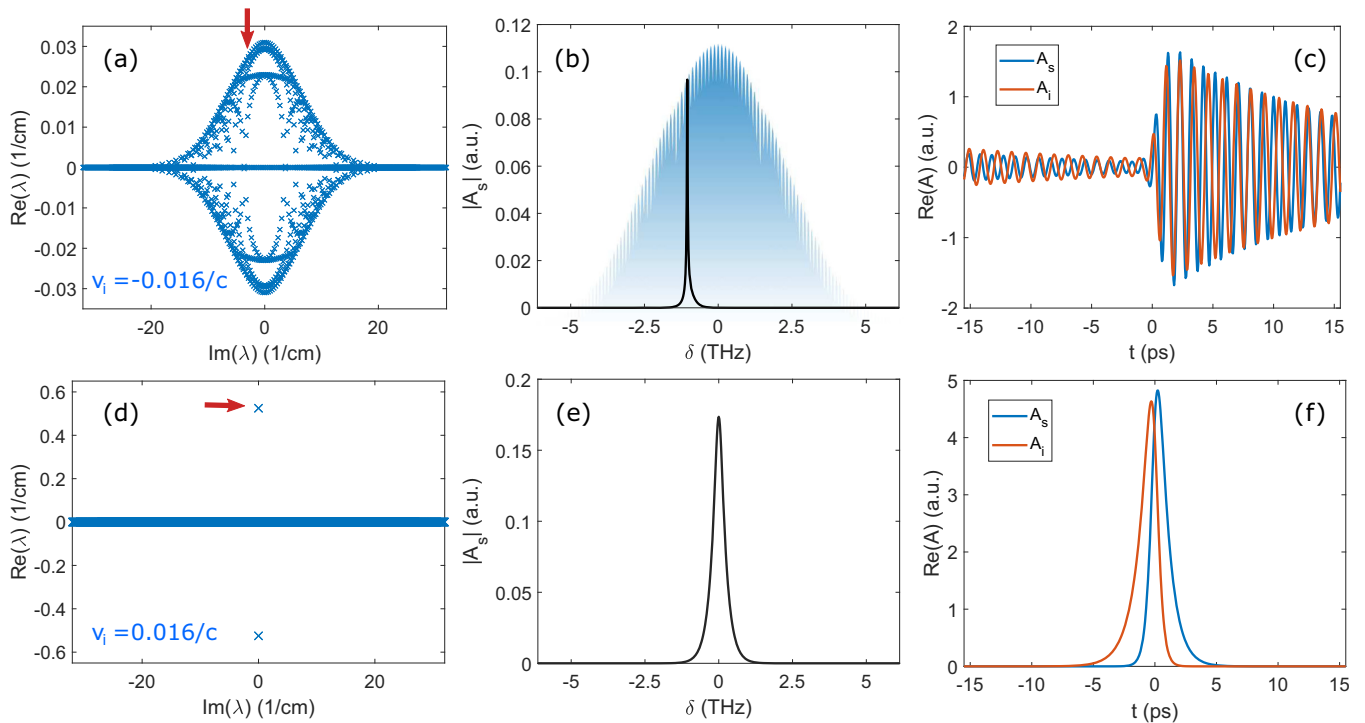


FIG. 2. Spectrum and unstable eigenvectors of Eq. (12) for  $P = 0.25$  W,  $T = 0.5$  ps, and different combinations of GVM parameters: (a)–(c)  $v_s = 0.013/c$ ,  $v_i = -0.016/c$ ; and (d)–(f)  $v_s = 0.013/c$ ,  $v_i = 0.016/c$ . (a) and (d) show eigenvalues calculated using numerical discretization with  $N = 1024$  Fourier modes. Spectra of the signal field corresponding to particular eigenvalues, indicated with red arrows in (a) and (d), are plotted in panels (b) and (e), respectively. The shaded area in (b) shows the combined spectrum of all signal components of unstable perturbations (see the main text for details). Panels (c) and (f) show the corresponding mode profiles in time domain.

eigenvector and eigenvalue corresponding to the trapped state are given by

$$\lambda = g = \left( \sqrt{\frac{P}{P_{\text{th}}}} - 1 \right) \frac{v_s v_i}{2T v_+}, \quad (14a)$$

$$a_s(t) = \sqrt{v_i} \frac{\exp\{-t/\tilde{T} + t/2T\}}{\cosh^m(t/T)}, \quad (14b)$$

$$a_i(t) = \sqrt{v_s} \frac{\exp\{-t/\tilde{T} - t/2T\}}{i \cosh^m(t/T)}, \quad (14c)$$

$$P_{\text{th}} = \frac{v_s v_i}{4\gamma_2^2 T^2}, \quad \tilde{T} = \frac{v_s v_i}{g v_-}, \quad m = \frac{1}{2} \sqrt{\frac{P}{P_{\text{th}}}}, \quad (14d)$$

where  $v_{\pm}$  are defined in Eq. (4) and  $v_s v_i > 0$ . These solutions match the ones in Fig. 2(f) exactly. The trapping effect happens over the propagation distances shorter than the distance at which energies of the signal and idler become large enough to degrade the pump significantly, typically multiples of  $1/g$ .

Parametric gain threshold  $g = 0$  is exceeded for  $P > P_{\text{th}}$ . For our geometry and  $T = 0.5$  ps, the value of  $P_{\text{th}}$  is  $P_{\text{th}} = 0.15$  W.  $P_{\text{th}}$  can be found from the balance condition between the GVM and the  $\chi^{(2)}$  lengths. Indeed, resolving

$$L_{2nl} = 2L_{\text{gvm}} \quad (15)$$

relative to  $P$  yields  $P_{\text{th}}$ , see Eqs. (8) and (9). This remarkable result implies that the three bright pulses with substantially different group velocities can form a transient but long-living state sustained by a balance between the second-order nonlinearity and group-velocity mismatch. Before we move onto analysis of the propagation of trapped states, it will be insightful to formalize the stationary-pump approximation used to derive Eq. (12).

### B. Stationary-pump approximation

The analytical result in Eq. (14a) allows us to formulate the limits of validity of the stationary-pump approximation quite comprehensively. Requiring that the parametric gain length  $L_g = R/2g$  needed to achieve the signal amplification ratio  $R = \ln(|A_s^{\text{out}}|^2/|A_s^{\text{in}}|^2) > 1$  is smaller than the Kerr nonlinear length  $L_{3nl}$ , i.e.,  $L_g < L_{3nl}$ , we obtain

$$T > \frac{R}{1 - (2R\sqrt{P/P_{\text{nl}}} - 1)^2} T_{nl}, \quad (16)$$

$$P_{\text{nl}} = \frac{4\gamma_2^2 v_s v_i}{\gamma_{3pp}^2 v_+^2}, \quad T_{nl} = \frac{\gamma_{3pp} v_+}{\gamma_2^2}.$$

Similarly, requiring that the gain length is smaller than the dispersion length of the pump  $L_g < L_d$ , we obtain

$$\sqrt{\frac{P}{P_{\text{nl}}}} > \frac{T_{nl}}{4T} \left[ 1 + \frac{RT_d}{T} \right], \quad (17)$$

$$T_d = \frac{|\beta_{2p}| v_+}{v_s v_i}.$$

Conditions in Eqs. (16) and (17) together define a domain on the plane of parameters  $(P, T)$  of the input pulse, see shading in Figs. 3(a) and 3(b). The  $L_g = L_{3nl}$  (red line) and  $L_g = L_d$  (black line) curves intersect when  $L_d = L_{3nl}$ , see

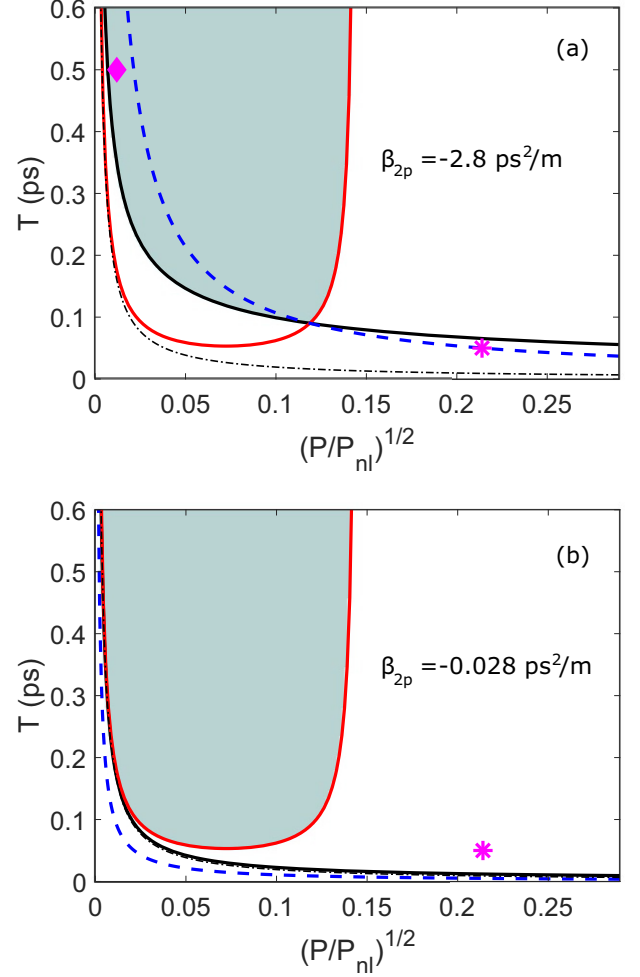


FIG. 3. Full-red (light gray) and black lines show the  $T$  vs  $P$  as given by Eqs. (16) and (17), respectively, for  $R = \ln(10^3)$ . Dashed-dotted line in (a) shows the parametric threshold  $T$  vs  $P_{\text{th}}$ . The same threshold practically merges with the full-black line in (b). Dashed blue lines show the  $T$  vs  $P_0$  for the soliton pulses, see Eq. (18). For the chosen waveguide geometry,  $P_{\text{nl}} = 3.1$  kW and  $T_{\text{nl}} = 8.5$  fs.

Fig. 3(a). The intersection point defines the minimal pulse duration satisfying the stationary-pump approximation,

$$T_{\text{min}} = \frac{R}{\sqrt{P_0/P_{\text{th}}} - 1} T_d, \quad (18)$$

$$P_0 = \frac{|\beta_{2p}|}{\gamma_{3pp} T^2}.$$

If the intersection does not occur, then the validity range of the stationary pump approximation is defined by the red line, i.e., by Eq. (16), with  $T_{\text{min}} = RT_{nl}$ , see Fig. 3(b). A special case of the stationary pump pulse profile is when it forms a soliton. This case deserves a separate consideration, see Sec. III E below.

### C. Dynamics of fundamental trapped states

We now choose a point where the stationary-pump approximation is predicted to work and describe a series of numerical simulations of Eq. (1) illustrating emergence and



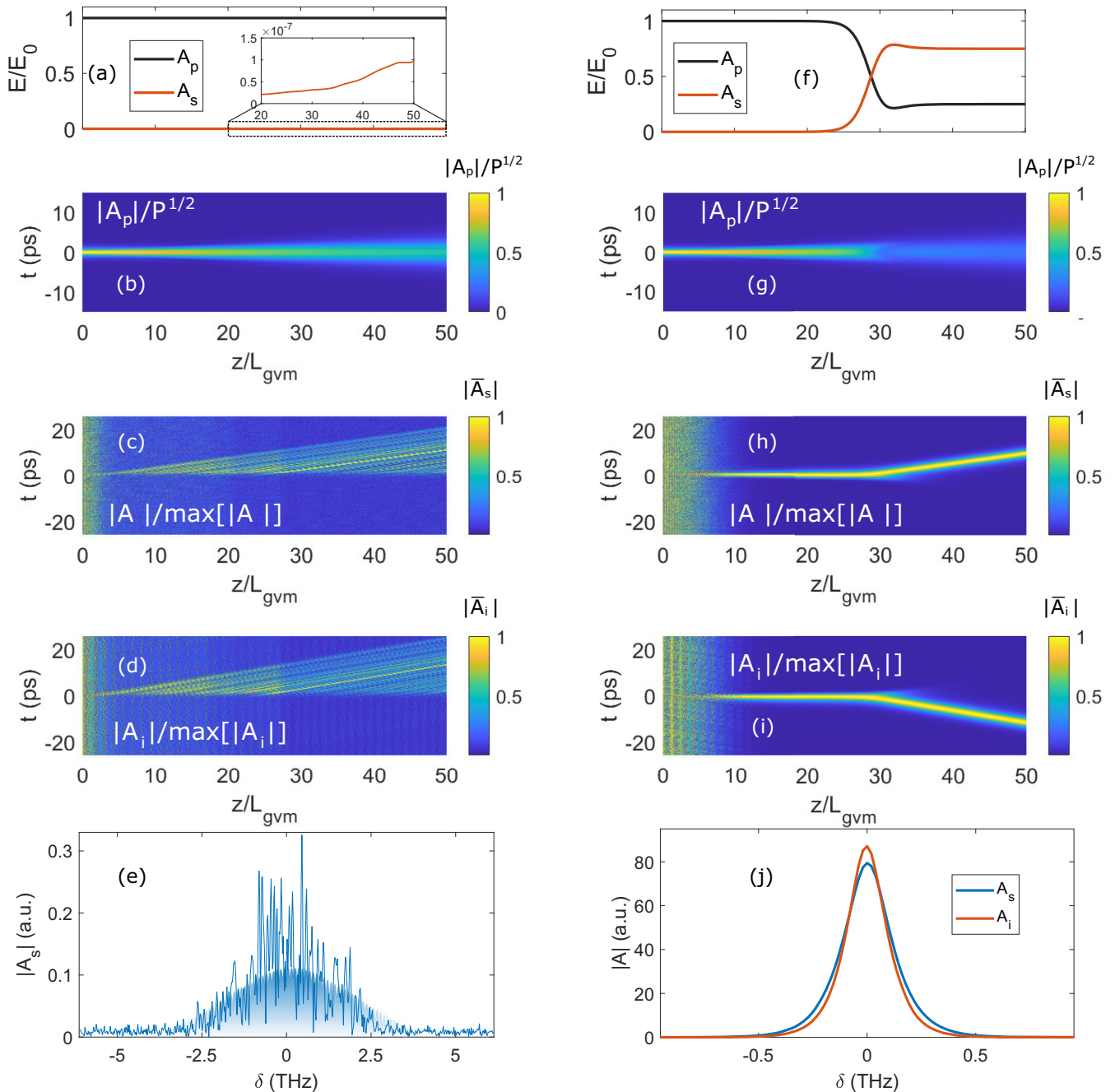


FIG. 4. Numerical simulation of the parametric conversion for  $P = 0.25$  W,  $T = 0.5$  ps, and spectrally uniform initial noise  $\sim 10^{-5}\sqrt{P}$ , in the signal and idler fields. Panels (a)–(e) correspond to  $v_i = -0.016/c$ , panels (f)–(j) correspond to  $v_i = 0.016/c$ . The signal GVM is  $v_s = 0.013/c$  in all cases. With these parameters, the GMV length is  $L_{\text{gvm}} \approx 1$  cm. Panels (a) and (f) show fractional total energy in the pump and signal fields, where  $E_0$  is the total energy of the input pump,  $E = \int |F|^2 dt$ ,  $F$  is either the pump or the signal field. The inset in (a) shows a zoomed part of the signal energy plot. Space-time dynamics of the pump and normalized signal and idler fields,  $\bar{A} = A/\max[|A|]$  are shown in panels (b)–(d) for  $v_i v_s < 0$  and in (g)–(i) for  $v_i v_s > 0$ . Panels (e) and (j) show the output spectra. The shaded region in (e) indicates the predicted gain spectrum computed using the eigenvalue problem in Eq. (12)

evolution of the signal and idler pulses. Changeover between trapping  $v_s v_i > 0$  and no-trapping  $v_s v_i < 0$ , conditions makes a profound impact on the observed spatiotemporal evolution and generated spectra, see Fig. 4. We fixed  $|v_s| = 0.016/c$ ,  $|v_i| = 0.013/c$ , and used the pump with  $P = 0.25$  W and  $T = 0.5$  ps ( $L_{\text{gvm}} \approx 1$  cm), see the rhombus in Fig. 3(a). Uniform random noise of a small amplitude  $|A| = 10^{-5}\sqrt{P}$  was

added in the signal and idler fields to trigger the parametric amplification processes. For  $v_s v_i < 0$  (left column of Fig. 4), we observe amplification of the signal-idler noise with the spectral bandwidth predicted by the eigenvalue analysis, cf. Figs. 2(b) and 4(e). The generated signal and idler waves are continuously emitted away from the pump because they have different group velocities determined by the linear dispersion,

see Figs. 4(c) and 4(d). Due to dispersion of the pump pulse, amplification of the signal and idler saturates at  $z \approx 47L_{\text{gvm}}$ , see Figs. 4(a) and 4(b).

For  $v_s v_i > 0$  (right column of Fig. 4), the nature of parametric conversion becomes qualitatively different. Now, parametric amplification leads to the emergence of localized signal-idler pulses trapped by the pump pulses and copropagating with it despite large GVM. This trapping is associated with the 20-fold amplification rate boost, cf. Figs. 2(a) and 2(d). Transfer of energy to the signal and idler stops due to pump depletion at  $z \approx 30L_{\text{gvm}}$ , when trapped signal and idler pulses are released abruptly and start propagating with their own group velocities, see Figs. 4(h) and 4(i). At this stage, nearly 80% of the initial pump energy has been already transferred to the signal and idler.

The signal and idler pulses in the fundamental trapped state and corresponding parametric gain are shown in the left inset and with the black line in Fig. 5(a), respectively. Maxima of the signal and idler pulses are shifted away from the pump center through the impact of the exponents in the numerators of Eqs. (14b) and (14c), see the left inset in Fig. 5(a) and Appendix C.

#### D. Higher-order trapped states

Increasing the pump peak power and/or pulse duration, and solving the eigenvalue problem Eq. (12), we have found higher-order trapped states, see Fig. 5(a). Our numerical results demonstrate that, similarly to the fundamental trapped state, gain of the higher-order states also increases linearly with  $\sqrt{P}$ . The thresholds for the  $n$ th-order state appear to satisfy  $P_{\text{th}}^{(n)} = (2n + 1)P_{\text{th}}$ , see Eq. (14d). We note that when the higher-order states' field crosses zero, its phase jumps by  $\pi$ .

Having the largest gain and lowest threshold, the fundamental state dominates the parametric generation. To illustrate this, we performed numerical simulations with a weak initial signal pulse consisting of many trapped states and pump power able to sustain all of them. To achieve the multimode excitation, we applied the seeded signal pulse detuned in frequency and delayed in time relative to the pump pulse:  $A_s(t, z = 0) \sim \text{sech}[(t - t_s)/T] \exp(-i\delta_s t)$ , whereas, the idler was set to zero. Pump power  $P = 10P_{\text{th}} = 1.5$  W and duration  $T = 0.5$  ps, were such that the eigenvalue analysis predicted coexistence of five trapped states,  $n = 0-4$ . Evolution of the signal field in time and frequency domains is shown in Figs. 5(b) and 5(c).

Calculated projections of the signal and idler onto all five trapped states are shown in Fig. 5(d). The initial signal pulse had a large proportion of the higher-order trapped states. However, since the higher-order states have lower gain, the fundamental state comes out as the dominant one already at  $z \gtrsim 0.4L_{\text{gvm}}$ . This dynamical re-ordering of the power of trapped states is also reflected in the changes in the temporal and spectral pulse profiles at  $z \approx 0.5L_{\text{gvm}}$  in Figs. 5(b) and 5(c).

#### E. Soliton pump

If the pump dispersion is anomalous,  $\beta_{2p} < 0$ , then the pump pulse can form a soliton. The soliton peak power  $P_0$

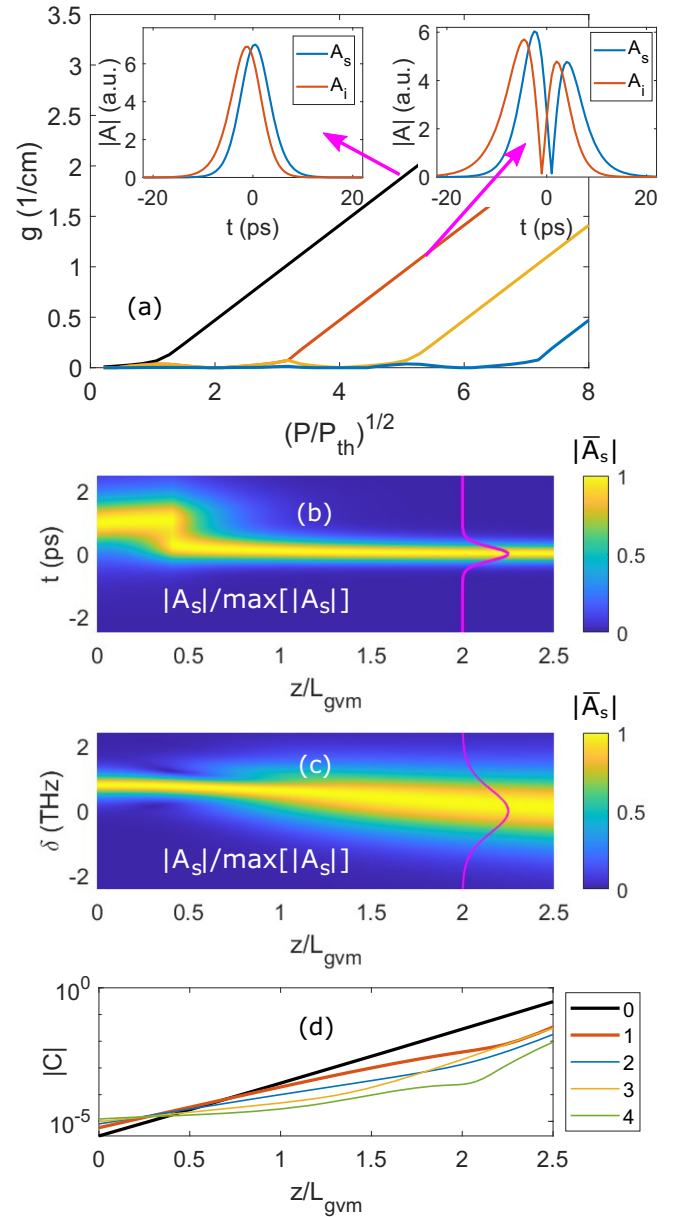


FIG. 5. (a) Gain vs pump power  $P$  for the first four trapped states  $T = 0.5$  ps. The insets illustrate profiles of the fundamental and first-order trapped states at  $P = 0.75$  W ( $P = 5P_{\text{th}}$ ). In the first-order state, the phases of each field jump by  $\pi$  at the nodal intensity points located in a vicinity of  $t = 0$  ps; (b)–(d) Parametric amplification with  $P = 1.5$  W ( $P = 10P_{\text{th}}$ ) and an initial small-amplitude localized pulse in signal field, shifted in frequency and position relative to the pump pulse by  $t_s = 1$  ps and  $\delta_s = 0.8$  THz. (b) is the time profile and (c) is the spectral evolution along the waveguide length. Time profile and spectrum of the signal component of the fundamental state are indicated with the pink/gray lines. (d) shows the projection coefficients onto the five trapped modes vs the propagation distance.

and duration  $T$  are connected exactly as per the second line of Eq. (18), see the dashed blue lines in Fig. 3. Using the soliton pump allows to boost conversion efficiency further. To illustrate this, we compared conversion efficiencies for the nonsoliton and soliton pulses, see the pink stars in Figs. 3(b) and 3(a), respectively. In both cases, the pump pulse duration

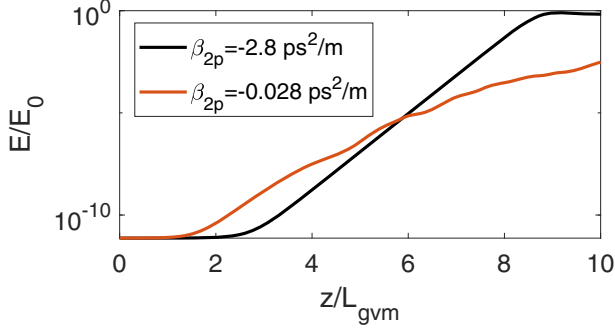


FIG. 6. Energy of the signal field  $E$ , as a fraction of the input pump energy  $E_0$ . Initial spectrally uniform noise of the amplitude  $|A| \sim 10^{-5}\sqrt{P}$  was added to the signal and idler fields. Pump pulse duration  $T = 0.05$  ps corresponds to  $L_{\text{gvm}} \approx 1$  mm. Power  $P = 170$  W corresponds to the solitonic and nonsolitonic pump pulses for  $\beta_{2p} = -2.8$  ps<sup>2</sup>/m and  $\beta_{2p} = -0.028$  ps<sup>2</sup>/m cases, respectively. Also, see pink stars in Figs. 3(a) and 3(b).

to  $T = 0.05$  ps and power  $P = 170$  W. Figure 6 compares how energy of the signal pulse is growing with the propagation distance in these two cases. The nonsolitonic regime (red line) leads to the dramatically suppressed conversion efficiency compared to the soliton case (black line). This is due to the considerable self-phase modulation and dispersion of the pump in the former case.

The soliton has the power-dependent phase,

$$A_p = \sqrt{P_0} e^{iqz} \text{sech}(t/T), \quad q = \frac{1}{2} P_0 \gamma_{3pp}, \quad (19)$$

and introduces the strong cross-phase modulation effect on the signal and idler fields. Using Eq. (6), and introducing

$$\begin{aligned} A_s(t, z) &= e^{(\lambda+iq/2)z} a_s(t), \\ A_i(t, z) &= e^{(\lambda^*-iq/2)z} a_i^*(t), \end{aligned} \quad (20)$$

we find a more complex eigenvalue problem,

$$\begin{aligned} \lambda \begin{bmatrix} a_s \\ a_i \end{bmatrix} &= \begin{bmatrix} \widehat{D}_s & i\gamma_2 S \\ -i\gamma_2 S & \widehat{D}_i^* \end{bmatrix} \begin{bmatrix} a_s \\ a_i \end{bmatrix}, \\ \widehat{D}_s &= -i\frac{1}{2}q - v_s \partial_t + i2\gamma_{3ps} S_0^2, \\ \widehat{D}_i &= -i\frac{1}{2}q + v_i \partial_t + i2\gamma_{3pi} S_0^2, \\ S_0 &= \sqrt{P_0} \text{sech}(t/T). \end{aligned} \quad (21)$$

Here, dispersion of the signal and idler fields can still be neglected assuming that the GVM is strongly dominant. For a particular relationship between the signal and the idler cross-phase modulation coefficients,  $\gamma_{3ps}/v_s = \gamma_{3pi}/v_i$ , we found the analytical expressions for the fundamental trapped state, see Appendix D,

$$\begin{aligned} a_{s,i}^{\text{sol}}(t) &= a_{s,i}(t) \exp \left\{ i\phi(t) - \frac{i|\beta_{2p}|}{4T^2 v_+} t \right\}, \\ \phi(t) &= \frac{|\beta_{2p}|}{\gamma_{3pp} T} \left( \frac{\gamma_{3ps}}{v_s} + \frac{\gamma_{3pi}}{v_i} \right) \tanh \left( \frac{t}{T} \right), \end{aligned} \quad (22)$$

Soliton-induced parametric gain,  $g = \text{Re}(\lambda)$ , is the same as in Eq. (14).

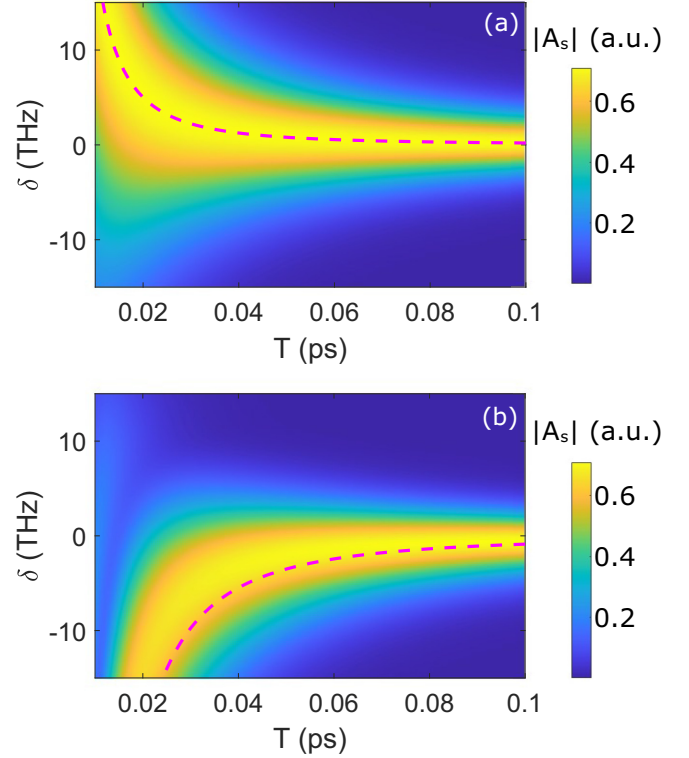


FIG. 7. Spectrum of the trapped mode (signal component) as a function of the soliton pump pulse width for (a)  $\gamma_{3ps} = (v_s/v_i)\gamma_{3pi} = 0.09$  W<sup>-1</sup>m<sup>-1</sup>; (b)  $\gamma_{3ps} = (v_s/v_i)\gamma_{3pi} = 4.5$  W<sup>-1</sup>m<sup>-1</sup>. Dashed lines show the predicted frequency shifts using Eq. (23).

Leaving the intensity profiles of the trapped states unaffected, cross-phase modulation induces a frequency chirp via the time-dependent phase  $\phi(t)$ . The associated instantaneous frequency shift  $\delta_c = -\partial_t \phi(t)$  is always negative for the signal and positive for the idler, see the complex conjugate  $a_i$  in Eq. (20). The other frequency shift  $\delta_0 = |\beta_{2p}|/4T^2 v_+$  is associated with the modified phase-matching condition due to self-phase modulation of the pump, and it acts in the opposite direction for  $v_+ > 0$ . The net shift  $\delta = \delta_c + \delta_0$  depends on the balance between the cross-Kerr and self-Kerr effects. Particularly, at  $t = 0$ , where  $\delta_c$  has its maximal value, the net frequency shift is

$$\delta = \frac{|\beta_{2p}|}{4v_+ T^2} \left[ 1 - \frac{4v_+}{\gamma_{3pp}} \left( \frac{\gamma_{3ps}}{v_s} + \frac{\gamma_{3pi}}{v_i} \right) \right]. \quad (23)$$

When the cross-Kerr coefficients are small,  $\gamma_{3ps} v_+ / \gamma_{3pp} v_s \ll 1$ ,  $\gamma_{3pi} v_+ / \gamma_{3pp} v_i \ll 1$ , the net  $\delta$  is positive, see Fig. 7(a), which corresponds to the signal and idler carrier frequencies  $\omega_s$  and  $\omega_i$ , experiencing blueshifts and redshifts, respectively. However, when the cross-Kerr effect is relatively strong, the net shift is negative, see Fig. 7(b), so that now the signal becomes redder and the idler becomes bluer.

#### IV. SUMMARY AND DISCUSSION

We have developed a detailed theory of the signal and idler trappings by the ultrashort pump pulse generating parametric gain in a material with second- and third-order nonlinearities. We have derived explicit analytical solutions for the trapped

states in the cases of stationary-pump approximation and soliton pump. We have revealed that the trapping takes place when, e.g., the signal is slower than the pump, and the idler is faster and vice versa, and at the same time, the characteristic length corresponding to the pulse walk-off is matched to half of the nonlinear length. We have demonstrated that the trapping to the no-trapping transition leads to the change over between the broadband coherent and the in-coherent signal and idler spectra. In the coherent case, spectral peaks of the signal and idler pulses are further shifted in the opposite direction via the Kerr nonlinearity-induced cross-phase modulation effect.

The importance of the trapping effect for applications come through the dramatic increase in the conversion efficiency and through the emerging application for frequency conversion of the optical frequency combs [28–30]. We expect a similar trapping phenomenon to happen in the nondegenerate four-wave-mixing frequency conversion in the absence of second-order nonlinearity [21].

Since the signal and idler frequencies in three-wave mixing processes are located relatively close to each other and are well separated from the pump, one could expect that the trapping condition  $v_s v_i > 0$  implies that between the signal and the idler frequencies, there should be a point where group velocity is matched to the pump group velocity. One way this can happen is when dispersions of the pump and signal/idler are of the opposite signs, which also underpins the radiation trapping effect driving supercontinuum expansion in photonic crystal fibers [14].

### ACKNOWLEDGMENT

This work was supported by the Royal Society (Grant No. IES/R3/223225).

We declare no conflicts of interest. Data included in this paper are openly available [31].

### APPENDIX A: NONLINEAR COEFFICIENTS

The field amplitudes in Eq. (1) are normalized such that  $(\omega_k/\omega_p)|A_k|^2$  gives power in watts,  $k = p, s,$  and  $i$ . The nonlinear coefficients are calculated using the methodology of Refs. [32–34],

$$\gamma_2 = \frac{\epsilon_0 \sqrt{\omega_s \omega_i}}{4 \sqrt{N_s N_i N_p}} \iint \vec{e}_p^* \hat{\chi}_2(x, y) \cdots \vec{e}_s \vec{e}_i dx dy, \quad (\text{A1})$$

$$\gamma_{3kj} = \frac{1}{\omega_p} \frac{\epsilon_0 \omega_k \omega_j}{16 N_k N_j} \iint \vec{e}_j^* \hat{\chi}_3(x, y) \cdots \vec{e}_k \vec{e}_k^* \vec{e}_j dx dy, \quad (\text{A2})$$

$$N_k = \frac{1}{4} \iint (\vec{e}_k \times \vec{h}_k^* + \vec{e}_k^* \times \vec{h}_k) \cdot \vec{z} dx dy, \quad (\text{A3})$$

where  $\vec{e}_k(x, y)$  and  $\vec{h}_k(x, y)$  are electric- and magnetic-field profiles of the pump, signal, and idler modes,  $\hat{\chi}_2(x, y)$  and  $\hat{\chi}_3(x, y)$  are material nonlinearity tensors,  $\vec{z}$  is the unit vector along the propagation direction  $z$ .

In the case of a weakly guiding structure (i.e., when the longitudinal components of the fields are negligible), the

normalization factors in Eq. (A3) can be approximated as

$$N_k \approx \frac{c \beta_k}{2 Z_0 \omega_k} \iint |\vec{e}_k|^2 dx dy, \quad (\text{A4})$$

where  $Z_0 = 1/(\epsilon_0 c)$  is the vacuum impedance.

### APPENDIX B: PARAMETRIC GAIN IN THE cw REGIME

For the case of a constant amplitude pump,  $S(t) = \sqrt{P_0} = \text{const.}$ , the spectrum of Eq. (12) can be found analytically using  $a_s, a_i \sim \exp(-i \delta t)$ ,

$$\lambda_{1,2}^{(\text{cw})} = i \frac{k_s(\delta) - k_i(-\delta)}{2} \pm \sqrt{\gamma_2^2 P_0 - \frac{1}{4} [k_s(\delta) + k_i(-\delta) - q]^2}, \quad (\text{B1})$$

where

$$k_s(\delta) = v_s \delta + \frac{\beta_{2s}}{2} \delta^2 + 2\gamma_{3ps} P_0, \quad (\text{B2})$$

$$k_i(\delta) = -v_i \delta + \frac{\beta_{2i}}{2} \delta^2 + 2\gamma_{3pi} P_0, \quad (\text{B3})$$

and  $\delta$  means detuning from the frequency  $\omega_s$  of the signal field (the corresponding detuning for the idler field is  $-\delta$ ).

Conditioning the square root to zero, one can find a range of  $\delta$ 's,  $\delta_1 < \delta < \delta_2$ , corresponding to the exponentially growing signal and idler, i.e.,  $\text{Re}[\lambda(\delta)] > 0$ . If

$$\Delta(\delta) = k_s(\delta) + k_i(-\delta) - q, \quad (\text{B4})$$

then  $\Delta(\delta_{1,2}) = \pm 2\gamma_2 \sqrt{P_0}$ . This is the modified phase-matching condition, which takes into account the shift of the pump propagation constant ( $q$ ), shifts of the signal/idler propagation constants due to frequency detunings and nonlinear corrections to the propagation constants due to the cross-phase modulation with the pump.

The expressions for  $\delta_{1,2}$  become particularly transparent when the second-order dispersion can be disregarded relative to the large walk-off,

$$\delta_{1,2} = \frac{q \pm \gamma_2 \sqrt{P_0}}{v_s + v_i}. \quad (\text{B5})$$

For a given combination of  $|v_s|$  and  $|v_i|$ , the gain bandwidth is broader when  $v_s v_i < 0$ . The maximal possible gain,  $\max[\text{Re}(\lambda)] = \gamma_2 \sqrt{P_0}$ , is achieved at the phase matching,

$$\Delta(\delta_m) = 0, \quad (\text{B6})$$

and it does not depend on the combination of  $v_s$  and  $v_i$ .

### APPENDIX C: FUNDAMENTAL TRAPPED STATE

For the sake of generality, we reinstate the pump propagation constant shift  $q$  in the eigenvalue problem in Eq. (12),

$$\lambda a_s = \left(-i \frac{q}{2} - v_s \partial_t\right) a_s + i \gamma_2 S(t) a_i, \quad (\text{C1})$$

$$\lambda a_i = \left(i \frac{q}{2} + v_i \partial_t\right) a_i - i \gamma_2 S(t) a_s. \quad (\text{C2})$$

Using the ansatz,

$$a_s(t) = e^{-i \delta_0 t} F(t/T), \quad (\text{C3})$$

$$a_i(t) = -i e^{-i \delta_0 t} H(t/T), \quad (\text{C4})$$



and splitting the eigenvalue  $\lambda$  into real and imaginary parts,

$$\lambda = g + i\kappa, \quad (\text{C5})$$

we obtain two coupled equations for  $\kappa$  and  $\delta_0$ ,

$$\kappa = -\frac{q}{2} + v_s \delta_0, \quad (\text{C6})$$

$$\kappa = \frac{q}{2} - v_i \delta_0, \quad (\text{C7})$$

and a separate set of equations for the real functions  $F$  and  $H$ ,

$$gF(\tau) = -(v_s/T)F'(\tau) + \gamma_2 S(\tau)H(\tau), \quad (\text{C8})$$

$$gH(\tau) = (v_i/T)H'(\tau) + \gamma_2 S(\tau)F(\tau), \quad (\text{C9})$$

where we use primes to denote derivatives in  $\tau = t/T$ :  $F' = dF/d\tau$ .

The first set of equations gives the frequency detuning and the imaginary part of the eigenvalue,

$$\delta_0 = \frac{q}{v_s + v_i} = \frac{q}{2v_+}, \quad (\text{C10})$$

$$\kappa = \frac{q(v_s - v_i)}{2(v_s + v_i)} = \frac{qv_-}{2v_+}. \quad (\text{C11})$$

To proceed with the solution of Eqs. (C8) and (C9), it is convenient to introduce a new function,

$$u(\tau) = \frac{F(\tau)}{H(\tau)} \quad (\text{C12})$$

for which the following differential equation is derived:

$$u' = -g\left(\frac{T}{v_s} + \frac{T}{v_i}\right)u + \gamma_2 S(\tau)\left(\frac{T}{v_s} + \frac{T}{v_i}u^2\right). \quad (\text{C13})$$

Using the pump function in Eq. (10), and introducing a rescaling,

$$u(\tau) = \sqrt{\frac{v_i}{v_s}} r(\tau), \quad (\text{C14})$$

we rewrite Eq. (C13) in the following form:

$$r' = \left[ -g\left(\frac{T}{v_s} + \frac{T}{v_i}\right) + \frac{2\gamma_2\sqrt{PT}}{\sqrt{v_s v_i}} \frac{r + r^{-1}}{e^\tau + e^{-\tau}} \right] r. \quad (\text{C15})$$

One can see that

$$r(\tau) = \sigma \exp(\pm\tau) \quad (\text{C16})$$

is the solution of the above equation with  $\sigma = \pm 1$ , provided the following condition is satisfied:

$$-g\frac{v_s + v_i}{v_s v_i} + \sigma \frac{2\gamma_2\sqrt{P}}{\sqrt{v_s v_i}} = \pm \frac{1}{T}, \quad (\text{C17})$$

which sets the real part of the eigenvalue  $g$  (gain). Altogether there are four combinations with different signs of  $\sigma$  and different signs of the right-hand side [corresponding to different signs of the argument of the exponent in Eq. (C16)].

Using the solution for  $r(\tau)$  in Eq. (C16) and the definitions in Eqs. (C14) and (C12) from Eq. (C9) we obtain

$$gH = (v_i/T)H' + \sigma \sqrt{\frac{v_i}{v_s}} \frac{2\gamma_2\sqrt{P}e^{\pm\tau}}{e^\tau + e^{-\tau}} H, \quad (\text{C18})$$

which can be rewritten as

$$H' = \left[ \frac{\lambda T}{v_i} - \sigma \frac{\gamma_2\sqrt{PT}}{\sqrt{v_s v_i}} \mp \sigma \frac{\gamma_2\sqrt{PT}}{\sqrt{v_s v_i}} \tanh(\tau) \right] H. \quad (\text{C19})$$

Here, the upper/lower sign of the last term corresponds to the upper/lower sign of the argument of the exponent in the solution for  $r(\tau)$  in Eq. (C16).

The general solution of Eq. (C19) is (up to a constant amplitude factor),

$$H(\tau) = \exp(\gamma\tau) \cosh^{-m}(\tau), \quad (\text{C20})$$

$$\gamma = \frac{gT}{v_i} - \sigma \frac{\gamma_2\sqrt{PT}}{\sqrt{v_s v_i}}, \quad (\text{C21})$$

$$m = \pm \sigma \frac{\gamma_2\sqrt{PT}}{\sqrt{v_s v_i}}. \quad (\text{C22})$$

For localized solutions we require  $m > 0$ , therefore, out of four combinations of the signs of  $\sigma$  and the argument of exponent in the solution for  $r(\tau)$  in Eq. (C16), only two correspond to localized modes:  $r_1(\tau) = \exp(\tau)$  and  $r_2(\tau) = -\exp(-\tau)$ . Using the first combination of signs in Eq. (C17) we obtain the spectrum,

$$g_1 = \left( \frac{2\gamma_2\sqrt{P}}{\sqrt{v_s v_i}} - \frac{1}{T} \right) \frac{v_s v_i}{v_s + v_i}, \quad (\text{C23})$$

and the corresponding mode is

$$H_1(\tau) = \exp(\gamma\tau) \cosh^{-m}(\tau), \quad (\text{C24})$$

$$F_1(\tau) = \sqrt{\frac{v_i}{v_s}} \exp(\tau) H_1(\tau), \quad (\text{C25})$$

$$\gamma = \frac{g_1 T}{v_i} - \frac{\gamma_2\sqrt{PT}}{\sqrt{v_s v_i}} = -\frac{1}{2} - \frac{g_1 v_- T}{v_i v_s}, \quad (\text{C26})$$

$$m = \frac{\gamma_2\sqrt{PT}}{\sqrt{v_s v_i}}. \quad (\text{C27})$$

The gain of this mode is positive, provided

$$\gamma_2\sqrt{PT} > \frac{1}{2}\sqrt{v_s v_i}. \quad (\text{C28})$$

(which gives  $m > 1/2$ ). Below this threshold,  $m \leq 1/2$  and the mode is no longer localized.

Similarly, choosing the second solution  $r_2(\tau)$ , we obtain

$$g_2 = -g_1, \quad (\text{C29})$$

$$H_2(\tau) = \exp(\gamma\tau) \cosh^{-m}(\tau), \quad (\text{C30})$$

$$F_2(\tau) = -\sqrt{\frac{v_i}{v_s}} \exp(\tau) H_2(\tau), \quad (\text{C31})$$

and the same  $\gamma$  and  $m$  parameters as for the first solution. This mode exponentially decays with the propagation distance (i.e., it is the conjugate pair of the first mode).

Above the threshold, signal and idler fields of the mode in Eqs. (C24)–(C27) are exponentially localized with the asymptotes,

$$a_s(t \rightarrow +\infty) \sim \exp\left[-\frac{(2m-1)v_i t}{v_s + v_i T}\right], \quad (\text{C32})$$

$$a_s(t \rightarrow -\infty) \sim \exp\left[\frac{2mv_s + v_i t}{v_s + v_i T}\right], \quad (\text{C33})$$

$$a_i(t \rightarrow +\infty) \sim \exp\left[-\frac{2mv_i + v_s t}{v_s + v_i T}\right], \quad (\text{C34})$$

$$a_i(t \rightarrow -\infty) \sim \exp\left[\frac{(2m-1)v_s t}{v_s + v_i T}\right]. \quad (\text{C35})$$

Maxima of the signal and idler pulses are shifted away from the pump center. Depending on the combination of GVM and pump parameters, they can be located on the different or on the same side from the maximum of the pump pulse,

$$t_{\text{peak},s} = T \operatorname{arctanh}\left[\frac{v_s - v_i + 1/m}{v_s + v_i}\right]. \quad (\text{C36})$$

$$t_{\text{peak},i} = T \operatorname{arctanh}\left[\frac{v_s - v_i - 1/m}{v_s + v_i}\right]. \quad (\text{C37})$$

Near the threshold  $m = 1/2$ , the asymmetry of the signal and idler pulses becomes more pronounced. At the threshold, the signal (idler) fields become delocalized in the  $t \rightarrow +\infty$  ( $t \rightarrow -\infty$ ) tails.

#### APPENDIX D: SIGNAL AND IDLER PHASES INDUCED BY THE SOLITON PUMP

Including the cross-Kerr terms, the eigenvalue problem in Eq. (21) now becomes

$$\lambda a_s = \left(-i\frac{q}{2} - v_s \partial_t\right) a_s + i\gamma_2 S(t) a_i + i2\gamma_{3\text{ps}} |S(t)|^2 a_s, \quad (\text{D1})$$

$$\lambda a_i = \left(i\frac{q}{2} + v_i \partial_t\right) a_i - i\gamma_2 S(t) a_s - i2\gamma_{3\text{pi}} |S(t)|^2 a_i. \quad (\text{D2})$$

We use ansatz,

$$a_{s,i}(t) = a_{s,i}^{(0)}(t) \exp[i\phi(t)], \quad (\text{D3})$$

$$\lambda = \lambda_0 + i\kappa, \quad (\text{D4})$$

where  $a_s^{(0)}(t)$ ,  $a_i^{(0)}(t)$ , and  $\lambda_0$  are the eigenfunctions and the eigenvalue for  $\gamma_{3\text{ps}} = \gamma_{3\text{pi}} = 0$ .

We obtain the following set of equations for  $\kappa$  and  $\phi(t)$ :

$$\phi' = \frac{2\gamma_{3\text{ps}}}{v_s} |S(t)|^2 - \frac{\kappa}{v_s}, \quad (\text{D5})$$

$$\phi' = \frac{2\gamma_{3\text{pi}}}{v_i} |S(t)|^2 + \frac{\kappa}{v_i}, \quad (\text{D6})$$

which has a solution if  $\gamma_{3\text{ps}}/v_s = \gamma_{3\text{pi}}/v_i$ ,

$$\kappa = 0, \quad (\text{D7})$$

$$\phi(t) = \left(\frac{\gamma_{3\text{ps}}}{v_s} + \frac{\gamma_{3\text{pi}}}{v_i}\right) \int_{-\infty}^t |S(t')|^2 dt'. \quad (\text{D8})$$

In particular, for the sech pump function as in Eq. (10) we obtain

$$\phi(t) = PT \left(\frac{\gamma_{3\text{ps}}}{v_s} + \frac{\gamma_{3\text{pi}}}{v_i}\right) \tanh\left(\frac{t}{T}\right). \quad (\text{D9})$$

- 
- [1] C. Couteau, Spontaneous parametric down-conversion, *Contemp. Phys.* **59**, 291 (2018).
- [2] C. Fabre and N. Treps, Modes and states in quantum optics, *Rev. Mod. Phys.* **92**, 035005 (2020).
- [3] M. Ebrahimzadeh, Parametric light generation, *Philos. Trans. R Soc., A* **361**, 2731 (2003).
- [4] G. Cerullo and S. De Silvestri, Ultrafast optical parametric amplifiers, *Rev. Sci. Instrum.* **74**, 1 (2003).
- [5] M. Nisoli, S. De Silvestri, V. Magni, O. Svelto, R. Danielius, A. Piskarskas, G. Valiulis, and A. Varanavicius, Highly efficient parametric conversion of femtosecond Ti: Sapphire laser pulses at 1 kHz, *Opt. Lett.* **19**, 1973 (1994).
- [6] C. Manzoni, G. Cirmi, D. Brida, S. De Silvestri, and G. Cerullo, Optical-parametric-generation process driven by femtosecond pulses: Timing and carrier-envelope phase properties, *Phys. Rev. A* **79**, 033818 (2009).
- [7] H. Linnenbank and S. Linden, High repetition rate femtosecond double pass optical parametric generator with more than 2 W tunable output in the NIR, *Opt. Express* **22**, 18072 (2014).
- [8] A. Aadhi and G. K. Samanta, High power, high repetition rate, tunable broadband mid-IR source based on single-pass optical parametric generation of a femtosecond laser, *Opt. Lett.* **42**, 2886 (2017).
- [9] D. T. Reid, J. Sun, T. P. Lamour, and T. I. FERREIRO, Advances in ultrafast optical parametric oscillators, *Laser Phys. Lett.* **8**, 8 (2011).
- [10] D. D. Hickstein, D. R. Carlson, H. Mundoor, J. B. Khurgin, K. Srinivasan, D. Westly, A. Kowligy, I. I. Smalyukh, S. A. Diddams and S. B. Papp, Self-organized nonlinear gratings for ultrafast nanophotonics, *Nat. Photonics* **13**, 494 (2019).
- [11] M. Jankowski, C. Langrock, B. Desiatov, A. Marandi, C. Wang, M. Zhang, C. R. Phillips, M. Loncar, and M. M. Fejer, Ultra-broadband nonlinear optics in nanophotonic periodically poled lithium niobate waveguides, *Optica* **7**, 40 (2020).
- [12] P. Margules, J. Moses, H. Suchowski, and G. Porat, Ultrafast adiabatic frequency conversion, *J. Phys. Photonics* **3**, 022011 (2021).
- [13] B. B. Zhou, A. Chong, F. W. Wise, and M. Bache, Ultrafast and Octave-Spanning Optical Nonlinearities from Strongly Phase-Mismatched Quadratic Interactions, *Phys. Rev. Lett.* **109**, 043902 (2012).
- [14] A. V. Gorbach and D. V. Skryabin, Light trapping in gravity-like potentials and expansion of supercontinuum spectra in photonic-crystal fibres, *Nat. Photonics* **1**, 653 (2007).
- [15] A. V. Gorbach and D. V. Skryabin, Theory of radiation trapping by the accelerating solitons in optical fibers, *Phys. Rev. A* **76**, 053803 (2007).

- [16] A. Kudlinski and A. Mussot, Visible cw-pumped supercontinuum, *Opt. Lett.* **33**, 2407 (2008).
- [17] A. Bendahmane, A. Mussot, M. Conforti, and A. Kudlinski, Observation of the stepwise blue shift of a dispersive wave preceding its trapping by a soliton, *Opt. Express* **23**, 16595 (2015).
- [18] M. Jankowski, N. Jornod, C. Langrock, B. Desiatov, A. Marandi, M. Loncar, and M. M. Fejer, Quasi-static optical parametric amplification, *Optica* **9**, 273 (2022).
- [19] D. V. Skryabin and A. V. Yulin, Theory of generation of new frequencies by mixing of solitons and dispersive waves in optical fibers, *Phys. Rev. E* **72**, 016619 (2005).
- [20] A. V. Gorbach, D. V. Skryabin, J. M. Stone, and J. C. Knight, Four-wave mixing of solitons with radiation and quasi-nondispersive wave packets at the short-wavelength edge of a supercontinuum, *Opt. Express* **14**, 9854 (2006).
- [21] W. P. Grice, A. B. U'Ren, and I. A. Walmsley, Eliminating frequency and space-time correlations in multiphoton states, *Phys. Rev. A* **64**, 063815 (2001).
- [22] P. J. Mosley, J. S. Lundeen, B. J. Smith, P. Wasylczyk, A. B. U'Ren, C. Silberhorn, and I. A. Walmsley, Heralded Generation of Ultrafast Single Photons in Pure Quantum States, *Phys. Rev. Lett.* **100**, 133601 (2008).
- [23] R. Yanagimoto, E. Ng, M. Jankowski, H. Mabuchi, and R. Hamerly, Temporal trapping: a route to strong coupling and deterministic optical quantum computation, *Optica* **9**, 1289 (2022).
- [24] A. P. Sukhorukov and A. K. Shchednova, Parametric amplification of light in the field of a modulated laser wave, *Zh. Exp. Teor. Fiziki* **60**, 1251 (1971) [*Sov. Phys. JETP* **33**, 677 (1971)].
- [25] Y. N. Karamzin and A. P. Sukhorukov, Mutual focusing of intense light-beams in media with quadratic nonlinearity, *Zh. Exp. Teor. Fiziki* **68**, 834 (1975) [*Sov. Phys. JETP* **41**, 414 (1975)].
- [26] W. E. Torruellas, Z. Wang, D. J. Hagan, E. W. Van Stryland, G. I. Stegeman, L. Torner, and C. R. Menyuk, Observation of Two-Dimensional Spatial Solitary Waves in a Quadratic Medium, *Phys. Rev. Lett.* **74**, 5036 (1995).
- [27] W. R. Rowe, A. V. Gorbach, and D. V. Skryabin, Solitons near avoided mode crossings in  $\chi^{(2)}$  nanowaveguides, *Phys. Rev. A* **104**, 053510 (2021).
- [28] M. Roiz, K. Kumar, J. Karhu, and M. Vainio, Simple method for mid-infrared optical frequency comb generation with dynamic offset frequency tuning featured, *APL Photonics* **6**, 026103 (2021).
- [29] M. Roiz, J. Y. Lai, J. Karhu, and M. Vainio, Mid-infrared frequency comb with 25 pJ threshold via CW-seeded optical parametric generation in nonlinear waveguide, *Opt. Lett.* **46**, 4037 (2021).
- [30] M. Roiz and M. Vainio, Versatile optical frequency combs based on multi-seeded femtosecond optical parametric generation, *Opt. Express* **30**, 17789 (2022).
- [31] Dataset related to the article Trapping of ultrashort pulses in non-degenerate parametric conversion, University of Bath Research Data Archive (2023), <https://doi.org/10.15125/BATH-01283>.
- [32] X. Zhao, A. V. Gorbach, and D. V. Skryabin, Dispersion of nonlinearity in subwavelength waveguides: derivation of pulse propagation equation and frequency conversion effects, *J. Opt. Soc. Am. B* **30**, 812 (2013).
- [33] A. V. Gorbach and E. Ivanov, Perturbation theory for graphene-integrated waveguides: Cubic nonlinearity and third-harmonic generation, *Phys. Rev. A* **94**, 013811 (2016).
- [34] L. Cai, A. V. Gorbach, Y. Wang, H. Hu, and W. Ding, Highly efficient broadband second harmonic generation mediated by mode hybridization and nonlinearity patterning in compact fiber-integrated lithium niobate nano-waveguides, *Sci. Rep.* **8**, 12478 (2018).